On relativistic discs and rings

W. Kley

Max-Planck-Society, Research Unit Gravitational Theory, Universität Jena, Max-Wien-Platz 1, D-07743 Jena, Germany

5 February 2008

ABSTRACT
Sequences of infinitesimally thin, uniformly rotating, self-gravitating relativistic discs with internal two-dimensional pressure have been constructed. It is shown that in weaker relativistic configurations the sequences undergo a continuous bifurcation from a disc to a ring structure, while in stronger relativistic cases the sequences terminate at the mass-shed limit where gravitational forces are exactly balanced by centrifugal forces.

Key words: gravitation – relativity – galaxies:structure.

1 INTRODUCTION

Relativistic, self-gravitating discs may have played an important role during the process of galaxy formation in the early universe. For example, they can be considered as possible predecessors of galaxies today that contain a massive black hole in their centre. Also, during the final evolution of a close binary system, consisting of two neutron stars, the orbit shrinks rapidly due to the emission of gravitational waves and the two stars merge finally into one object. Shortly after this coalescence, the system can be approximately described as a highly flattened disc-like structure which may display relativistic effects. These systems may then be modeled, in a simplified approach, by infinitesimally thin discs where the vertical variation has been averaged onto the midplane.

Uniformly rotating relativistic discs with zero internal pressure have been studied in detail by Bardeen & Wagoner (1971). Here an expansion method was used in which the problem was reduced to a set of ordinary differential equations, which were then solved numerically for the higher order corrections. Nevertheless, using this method, strongly relativistic disc structures could also be calculated accurately. Recently, the analytical solution of this problem in terms of integral equations was obtained (Neugebauer & Meinel 1993), which could subsequently be solved utilizing hyper-elliptic functions (Neugebauer & Meinel 1995). This solution represents the first analytic solution of a continuously extended rotating object in general relativity. In these approaches a given equation of state ($p = 0$) and rotation law (Ω =const.) are assumed, and the Einstein-equations are solved directly.

The method of mirror images is another frequently used option to construct models of relativistic discs. Here one begins with a known axisymmetric metric (e.g. Kerr), makes a cut in the upper half of the $\rho - z$ plane where ρ and z are cylindrical coordinates, and identifies the metric functions there with those of a symmetric cut in the lower half which joins the first at the $z = 0$ plane (see Pichon & Lynden-Bell 1996, and references therein). This method yields disc solutions where the corresponding matter properties, i.e. the energy-momentum surface distribution, must be inferred from the pasted solution after the two cuts have been identified. The method was first used for relativistic discs by Turakulov (1990).

It is known that, in the Newtonian limit, the uniformly rotating pressure-less dust disc is unstable to all perturbing modes (Binney & Tremaine 1987), a result which most likely carries over into the relativistic regime (Bardeen & Wagoner 1971). The addition of pressure tends to stabilize the disc. For Newtonian discs it was shown recently (Kley 1996) that uniformly rotating, pressurized discs undergo a continuous bifurcation process into a ring-like structure via a sequence of dumb-bell shaped equilibria. This process has its three-dimensional analogue in the bifurcation of rotating stars into rings (Eriguchi & Sugimoto 1981).

In this paper we generalize the relativistic zero-pressure disc solutions by imposing a given (polytropic) equation of state relating the surface pressure with the surface density. This pressure may be thought of as being generated by the random internal peculiar velocities in a galaxy, and it has a stabilizing effect. This work on the other hand also generalizes the Newtonian results on thin Maclaurin discs and their bifurcations to the relativistic case.

In Section 2, the relevant equations are given and the numerical method is outlined in Section 3. In Section 4 the results of the numerical computations are presented and in Section 5 we conclude.

2 BASIC EQUATIONS

2.1   Einstein equations

We shall treat the problem of an infinitesimally thin gaseous disc with internal pressure acting only in the plane of the disc. The problem is treated in full general relativity. The disc is assumed to rotate rigidly with the angular velocity Ω. We use a cylindrical coordinate system

$$x_1 = \rho,\ x_2 = z,\ x_3 = \varphi,\ x_4 = t \tag{1}$$

where the disc is located in the equatorial plane ($z = 0$). The line element is written in the form used by Bardeen & Wagoner (1971)

$$ds^2 = e^{2\mu}\left(d\rho^2 + dz^2\right) + \rho^2 B^2 e^{-2\nu}(d\varphi - \omega dt)^2 - e^{2\nu} dt^2. \tag{2}$$

This metric describes general axisymmetric and stationary configurations in general relativity. Four metric functions (μ, ν, B, and ω), which depend only on the coordinates ρ and z, have to be determined.

For the energy-momentum tensor we use the expression for an ideal gas. We assume relativistic units and set $G = c = 1$ in all formulae.

$$T_{ab} = (\epsilon + p)u_a u_b + p\left(g_{ab} - \frac{N_a N_b}{N^c N_c}\right), \tag{3}$$

with

$$N_a = \frac{\partial z}{\partial x^a} = (0, 1, 0, 0). \tag{4}$$

In equation (3), ϵ is the total mass-energy density and p is the gas pressure. These are three-dimensional quantities. The last term, containing a projection along the z-axis, has been introduced to ensure that the pressure acts only in the equatorial plane, i.e. the forces perpendicular to the disc (in the z-equation) vanish.

The four velocity in case of pure rotation (no radial or vertical motions) is given by

$$u^a = u^4(0, 0, \Omega, 1)$$

where Ω is the angular velocity as seen by an observer at infinity. Throughout this work we assume rigid rotation, and thus Ω is a constant. From the normalization of the four velocity ($u_a u^a = -1$) one obtains with the given metric

$$u^4 = \frac{e^{-\nu}}{(1 - v_\varphi^2)^{1/2}}, \tag{5}$$

where

$$v_\varphi = \rho B e^{-2\nu}(\Omega - \omega) \tag{6}$$

is the rotational velocity in the locally non-rotating frame of reference.

The Einstein equations $G_{ab} = 4\pi T_{ab}$ yield four second order partial differential equations for the four metric potentials (see also Bardeen & Wagoner 1971)

$$e^{-2\mu}\left[\frac{1}{B}\nabla(B\nabla\nu) - \frac{1}{2}e^{-4\nu}\rho^2 B^2 \nabla\omega \cdot \nabla\nu\right] =$$
$$4\pi\left[(\epsilon + p)\frac{1 + v_\varphi^2}{1 - v_\varphi^2} + p\right], \tag{7}$$

$$\frac{e^{-2(\nu+\mu)}}{2\rho B^2}\left[\nabla(\rho^2 B^3 \nabla\omega) - 4\rho^2 B^3 \nabla\nu \cdot \nabla\omega\right] =$$
$$-8\pi(\epsilon + p)v_\varphi\left(1 - v_\varphi^2\right)^{-1}, \tag{8}$$

$$\frac{e^{-2\mu}}{\rho B}\nabla(\rho\nabla B) = 8\pi p, \tag{9}$$

and

$$\frac{e^{-2\mu}}{2\rho B}\left[-4\rho B(\mu_{,\rho\rho} + \mu_{,zz}) + 4\nabla e^\nu \cdot \nabla(B\rho e^{-\nu}) +\right.$$
$$\left. e^{-4\nu}\rho^3 B^3 \nabla\omega \cdot \nabla\omega\right] = 8\pi\epsilon. \tag{10}$$

Here the ∇-operator is used in cylindrical coordinates (ρ, z).

Since the disc is located in the $z = 0$ plane, it can be treated mathematically as a boundary condition to the otherwise empty space. The above equations reduce in the case of a vacuum to

$$\nabla(\nabla\nu) = \frac{1}{2}\rho^2 B^2 e^{-4\nu}\nabla\omega \cdot \nabla\omega - \frac{1}{B}\nabla B \cdot \nabla\nu \tag{11}$$

$$\nabla(\rho^2 \nabla\omega) = -\frac{\rho^2}{a}\nabla a \cdot \nabla\omega, \tag{12}$$

$$\nabla(\rho\nabla B) = 0 \tag{13}$$

$$\Delta_c \mu = \frac{1}{4}\rho^2 B^2 e^{-4\nu}\nabla\omega \cdot \nabla\omega + \frac{1}{B}\nabla B \cdot \nabla\nu$$
$$- \nabla\nu \cdot \nabla\nu + \frac{1}{\rho}\frac{\partial\nu}{\partial\rho} \tag{14}$$

where Δ_c denotes the Cartesian Laplace operator (for the coordinates ρ, z), and

$$a := \frac{B^3}{e^{4\nu}}.$$

In the disc we define the two-dimensional total surface energy density σ, and the surface pressure P through

$$\epsilon = \sigma(\rho)\delta(z)e^{-2\mu}, \qquad p = P(\rho)\delta(z)e^{-2\mu}, \tag{15}$$

where $\delta(z)$ denotes the usual Dirac delta function.

The proper density and pressure in the disc are then given by

$$\sigma_P = \sigma e^{-\mu}, \qquad P_P = P e^{-\mu}. \tag{16}$$

From momentum and energy conservation $T^{ab}_{\ ;b} = 0$ we obtain the radial hydrostatic equation in the plane of the disc

$$P_{P,\rho} + (\sigma_P + P_P)U'_{,\rho} = 0, \tag{17}$$

where U' is defined through

$$e^{2U'} = \left(u^4\right)^2 = \left(1 - v_\varphi^2\right)^{-1} e^{-2\nu}.$$

In deriving (17) we assumed a constant rotation rate Ω.

The total angular momentum of the disc is given by

$$J = 2\pi \int_{\text{Disc}} (\sigma + P)\frac{v_\varphi}{1 - v_\varphi^2}e^{-2\nu}B^2\rho^2 d\rho \tag{18}$$

and the total gravitational mass by

$$M = 2\pi \int_{\text{Disc}} (\sigma + 2P)B\rho d\rho + 2\Omega J \tag{19}$$

2.2   Equation of state

To close the set of equations, thermodynamic relations have to be added. We present calculations for two different equations of state. In the first, more explorative, test case we assume a simple relation between the total proper surface energy density σ_P and the proper (surface) pressure P_P

$$P_{\rm p} = \sigma_{\rm p}^{\gamma}, \tag{20}$$

where γ denotes a polytropic exponent which is set to 3 for all models. This first equation of state has been used only for the non-rotating models.

For the non-rotating and all rotating models we assumed an equation of state that obeys, in analogy to three-dimensional configurations, an isentropic relation for the proper two-dimensional surface quantities

$$d\sigma_{\rm p} - \frac{\sigma_{\rm p} + P_{\rm p}}{\sigma_{\rm p}^0} \, d\sigma_{\rm p}^0 = 0, \tag{21}$$

where $\sigma_{\rm p}^0$ denotes the proper surface rest mass density. The the total surface density $\sigma_{\rm p}$ is given by

$$\sigma_{\rm p} = \sigma_{\rm p}^0 + \sigma_{\rm p}^{\rm i},$$

where $\sigma_{\rm p}^{\rm i}$ denotes the proper (surface) internal energy density. In both cases equation (17) can be integrated and yields the condition of hydrostatic equilibrium. For the isentropic case one obtains

$$e^{\nu} \sqrt{1 - v_{\varphi}^2} \, \frac{\sigma_{\rm p} + P_{\rm p}}{\sigma_{\rm p}^0} = const. \tag{22}$$

For the isentropic equation of state we assume further a polytropic relation

$$P_{\rm p} = K \left(\sigma_{\rm p}^0 \right)^{\gamma} = (\gamma - 1)\sigma_{\rm p}^{\rm i}. \tag{23}$$

In the non-relativistic limit the metric potential ν turns into the Newtonian potential and the hydrostatic equation reduces to the well known relation

$$\nu + \frac{\gamma}{\gamma - 1} \frac{P}{\sigma} - \frac{1}{2} r^2 \Omega^2 = const.$$

For $\gamma = 3$ there exists an analytic solution in the Newtonian limit, the Maclaurin disc solution (cf. Binney & Tremaine 1987). In this case the rotation rate Ω and the polytropic constant K are related through

$$\frac{K}{K_{\max}} = 1 - \left(\frac{\Omega}{\Omega_{\rm c}} \right)^2, \tag{24}$$

where $K_{\max}$ is the maximum value of K which is taken for zero rotation $\Omega = 0$, and $\Omega_{\rm c}$ is the maximum rotation rate for the pressure-less dust disc which has $K = 0$. The surface density is given by

$$\sigma(\rho) = \sigma_0 \sqrt{1 - (\rho/\rho_{\rm d})^2}, \tag{25}$$

where σ_0 denotes the central surface density of the disc and $\rho_{\rm d}$ is the disc radius.

2.3 Boundary conditions

In the equatorial plane ($z = 0$) the potentials are continuous. The presence of the disc however is given by jump conditions for the first derivatives of the metric potentials. By vertically integrating equations (7 to 10) the following jump conditions are obtained:

$$\nu_{,z} = 2\pi \left[(\sigma + P)\frac{1 + v_{\varphi}^2}{1 - v_{\varphi}^2} + P \right] \tag{26}$$

$$\omega_{,z} = -8\pi(\sigma + P)\frac{\Omega - \omega}{1 - v_{\varphi}^2} \tag{27}$$

$$\frac{B_{,z}}{B} = 4\pi P \tag{28}$$

$$\mu_{,z} = -2\pi\sigma. \tag{29}$$

These equations form the boundary conditions within the disc region $\rho < \rho_{\rm d}$. Outside, for $\rho > \rho_{\rm d}$ all vertical derivatives with respect to z vanish. On the polar axis ($\rho = 0, z > 0$) the radial derivatives of all potentials are zero. Because of local flatness the additional relation

$$B = e^{\nu + \mu} \tag{30}$$

holds on the axis, and will be used in obtaining the numerical solution. At infinity the potentials ν, ω, μ vanish, and $B = 1$.

3 METHOD OF SOLUTION

The vacuum Einstein equations (11-14), together with the boundary conditions (26 - 29) in the disc, form a very complicated set of non-linear partial differential equations and we resort to a numerical solution. As it is numerically inconvenient to work with boundary conditions at infinity, we first perform a coordinate transformation that takes infinity to a finite distance, say 1. Specifically, we transform the equations into the new coordinates u and v which are defined by:

$$u = \frac{\rho}{\rho + \rho_{\rm d}}, \quad \text{and} \quad v = \frac{z}{z + \rho_{\rm d}}. \tag{31}$$

The disc has the radius $u_{\rm d} = 0.5$ in these coordinates, which is held fixed in all models.

To obtain the actual numerical solution, the partial differential equations (11-14) are discretized on a suitable grid of $NU \times NV$ grid-cells. In the models presented here, a resolution of 128×128 grid-cells was used; only in the stronger relativistic cases was a higher resolution of 256×256 used. The radial grid-points are usually spaced equidistantly in physical space within the disc region $\rho < \rho_{\rm d}$ ($u < 0.5$) and equidistantly in u outside this region. The vertical grid-points are spaced equidistantly in v. Specifically, the first radial grid-point u_1 lies at $u = 0$ ($\rho = 0$) and the last one u_{NU+1} at $u = 1$ ($\rho = \infty$), and similarly for the v-coordinate. The discretization leads to a set of four coupled systems of linear equations which have a banded structure. The non-linear right hand sides of eqs. (11-14) are not linearised, but rather updated at each cycle during the process of iteratively solving the matrix-equations. This iterative solution of the matrix equations is obtained by the successive over relaxation (SOR) method, which is easy to program and allows a simple treatment of the boundary conditions.

The boundary conditions at infinity and on the axis are implemented straightforwardly. At infinity the values of ν, ω, and μ are set to zero and B is set to 1. On the axis and outside the disc the derivatives vanish which is implemented, for example, to second order in the grid spacing as

$$\nu_{1j} = (3\nu_{3j} - \nu_{2j})/4,$$

where the index j denotes the vertical grid-points. Only the actual jump conditions within the disc ($v = 0, u \leq u_{\rm d}$) have to be treated with more care. Starting from the minimum radius of the disc (ring) and then moving subsequently to larger values, the updated surface density is calculated from the hydrostatic equation (22) using the old values of the metric potentials. The jump conditions (26 - 29) are then used to obtain the new values of the potentials in the disc.
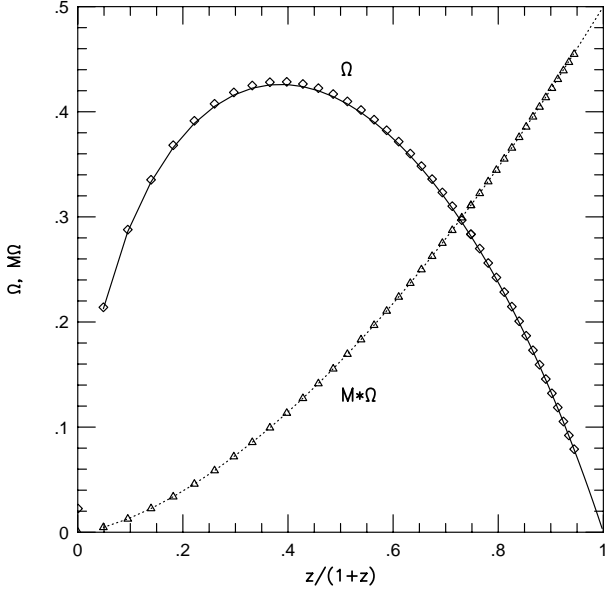
Figure 1. The angular velocity Ω and the total gravitational mass M as function of central redshift z for the pressure-less dust disc. The symbols refer to the numerical solution and the lines to the analytical solution.

Figure 2. Comparison of numerical and analytical results for three metric functions (see text) for the dust disc having a central redshift of $z = 2.97$. Lines refer to the analytical solution and symbols to the numerical solution. The radial coordinate ρ is given in units of the disc radius ρ_d.

Using this procedure, the boundary values are updated at each iteration cycle of the solver of the matrix equation.

The procedure of the solution depends on the type of solution sought. For the cases of disc and ring, and also for the intermediate 'dumb-bell' case which connects these two, slightly different methods have to be applied (see Kley 1996). In all cases the outer radius ρ_d of the configuration is held fixed at the value $u_\mathrm{d} = 0.5$ in dimensionless units. Additionally, the central potential $\nu_\mathrm{c} = \nu(0,0)$ is fixed during the iterations which is the equivalent of fixing the central redshift z, which is given by

$$z = \frac{1}{\sqrt{-g_{tt}(0,0)}} - 1. \tag{32}$$

where

$$g_{tt} = \left(\rho B e^{-\nu}\omega\right)^2 - e^{2\nu}. \tag{33}$$

The problem is then to determine the rotational angular velocity Ω and the pressure constant K simultaneously during the iterations. In the disc regime, either Ω or K can be fixed, and the other parameter can then be calculated from the hydrostatic equation (22). In the case of fixed Ω, the constant in (22) is fixed at the disc radius ρ_d and K is then obtained from evaluating (22) at the centre of the disc. In regions where $K(\Omega)$ may be double valued, which occurs in fact in the vicinity of the bifurcation to a dumb-bell sequence, it may be advantageous to switch the procedure and fix K. In this case Ω is calculated from (22) at a point within the disc, as at the origin the rotational velocity is zero. In the disc region both methods lead to the same results, which provides a good test for the internal consistency of the method. The latter method of holding K fixed during the iterations can in fact used up to that point at which the central density of the disc has reached zero. This dumb-bell region can also be calculated by fixing the central density $\sigma(0)$ and obtaining

Ω and K simultaneously from the hydrostatic equation (22) at two different locations. Again, this is consistent with the previous method. The dumb-bell part ends with a model which has zero central density at $\rho = 0$, and from here on the ring solutions continue. In this sequence, in addition to the outer radius ρ_d, the inner radius ρ_i of the ring is also held fixed. As before, K and Ω are obtained from the hydrostatics. The global accuracy of the method can be tested by comparing the asymptotic behaviour of ν and ω with the total mass and angular momentum of the disc. As the spherical radial coordinate $r = (\rho^2 + z^2)^{1/2} \rightarrow \infty$

$$\nu \quad \rightarrow \quad -\frac{M}{r} \tag{34}$$

$$\omega \quad \rightarrow \quad -2\frac{J}{r^3}. \tag{35}$$

Numerically, the evaluation of M and J at large distances agrees with the values obtained by integration over the disc (18) and (19), to within one percent. Only for stronger relativistic discs the agreement becomes weaker, due to the strong mass concentration in the centre of the disc. Additional test cases for the numerical method are presented below in the results section.

4   RESULTS

4.1   Test case: The pressure-less disc

Ideally, any newly developed numerical method needs to be tested against known analytical solutions. Fortunately, there exists a solution in the special case of a fully relativistic pressure-free disc (Neugebauer & Meinel 1993, 1995). A sequence of dust disc models were run with a varying central
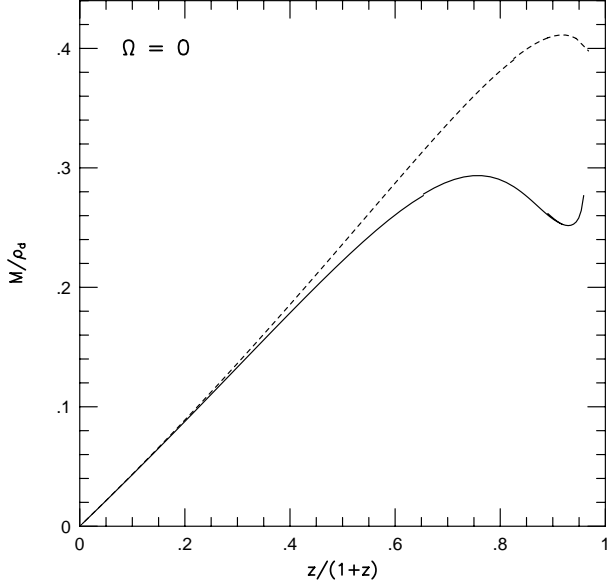
Figure 3. The total gravitational mass M versus central redshift for the non-rotating disc. The dashed lines refers to the equation of state (20) and the solid line to (23).
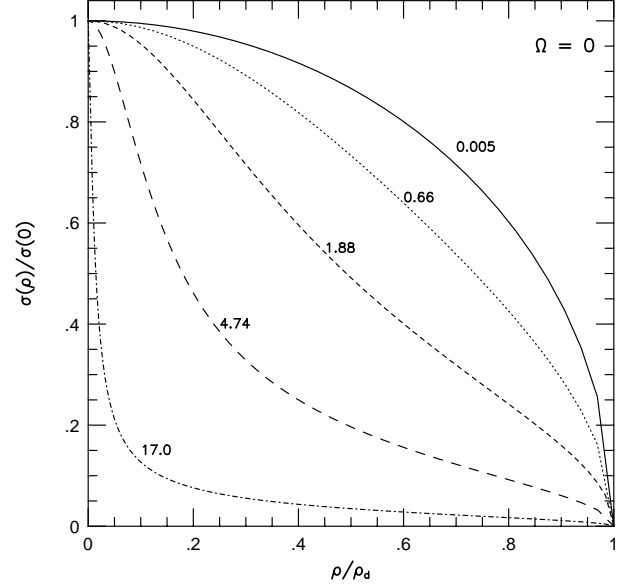

Figure 4. The normalized surface density σ as a function of radius for the non-rotating disc. The labels denote the value of the central redshift of the disc.

redshift. In Fig. 1 the angular velocity Ω (solid-line, diamonds) and the global quantity $M\Omega$ (dotted-line, triangles) are compared with the analytical solution for different central redshift z. The numerical and analytical solutions agree very well. Note that the angular velocity Ω is not a given fixed input parameter, but is determined self-consistently as a function of z (with fixed outer disc radius ρ_d) during the iterative solution. The normalized central redshift $z_n = z/(1 + z)$ serves as parameter which measures the strength of relativistic effects. In the Newtonian limit $z_n = 0$ and in the extreme relativistic limit $z_n = 1$. Locally, for the metric potentials, the agreement is very good as well. The metric potentials displayed in Fig. 2 are those of the line element written in Weyl-Lewis-Papapetrou form which has been used by Neugebauer & Meinel (1993). They are related to ν, ω, μ by

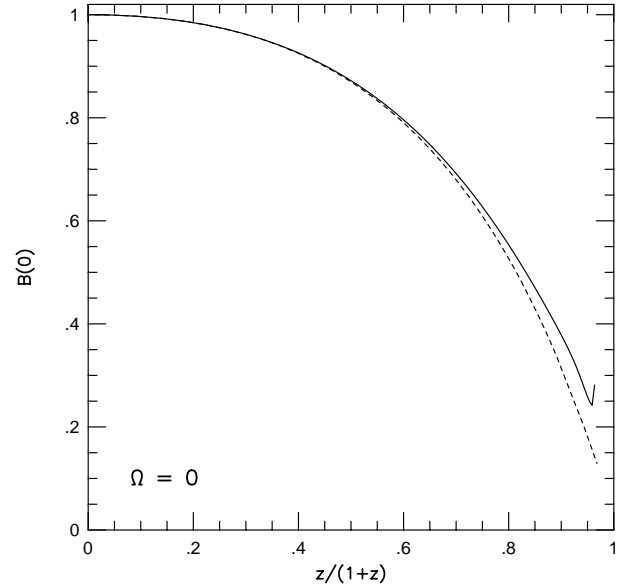$$e^{2U} = e^{2\nu} - \rho^2\omega^2 e^{-2\nu} \qquad (36)$$
$$ae^{2U} = \rho^2\omega e^{-2\nu} \qquad (37)$$
$$e^{2k} = e^{2(\nu+\mu)}. \qquad (38)$$

The potential B is equal to 1 everywhere for the dust disc. The results are compared for an intermediate redshift $z = 2.97$. For the general case, with internal pressure, there exists no analytical solution for a relativistic disc. In the Newtonian limit however, the numerically obtained solutions also agree very well with the known analytic Maclaurin disc solution (24, 25) and with the bifurcation diagrams found in the Newtonian case (Kley 1996). Although a complete test of the numerical approach was not possible, the test cases provide very positive indication as to the reliability of the results.

Figure 5. The central value of the potential B versus central redshift for the non-rotating disc for two different equations of state (see fig. 3).

4.2 Non-rotating discs

The non-rotating discs with $\Omega = 0$ are supported purely by internal pressure and have, for sequences of a given central redshift z, the maximum value of K. Similar to stars, non-rotating discs have a maximum mass M/ρ_d which increases with central redshift. In Fig. 3 the total gravitational mass is plotted versus central redshift for the two different equations of state. The higher total masses are reached in the case of the simple equation (20), dashed line, while the polytropic
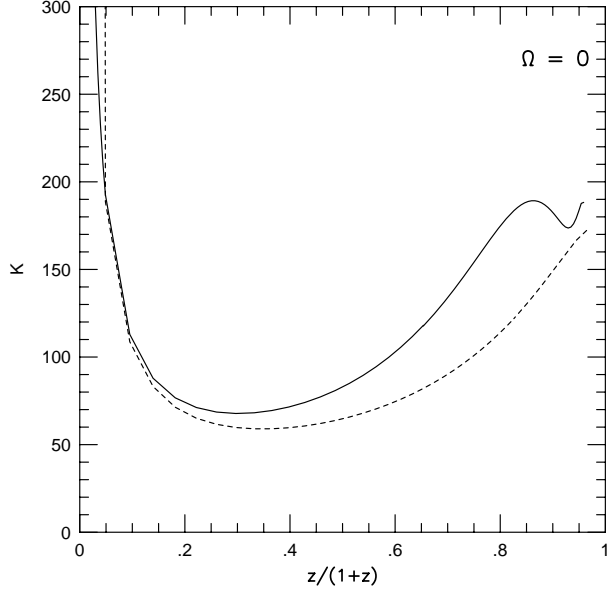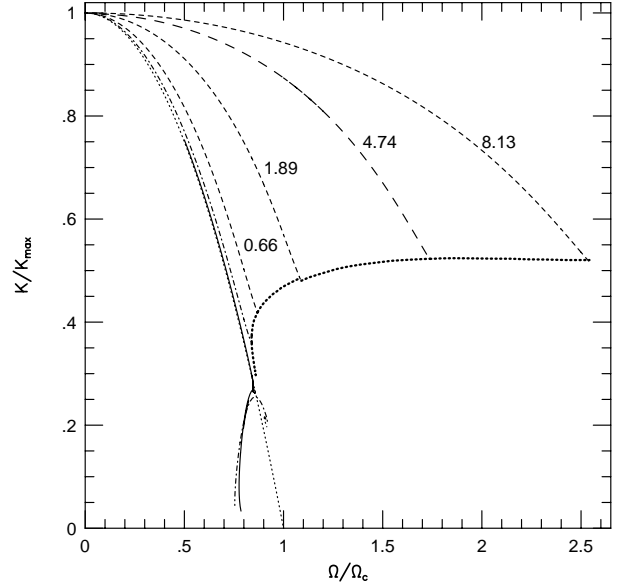
Figure 6. The polytropic constant K versus central redshift for the non-rotating disc for two different equations of state (see Fig. 3).
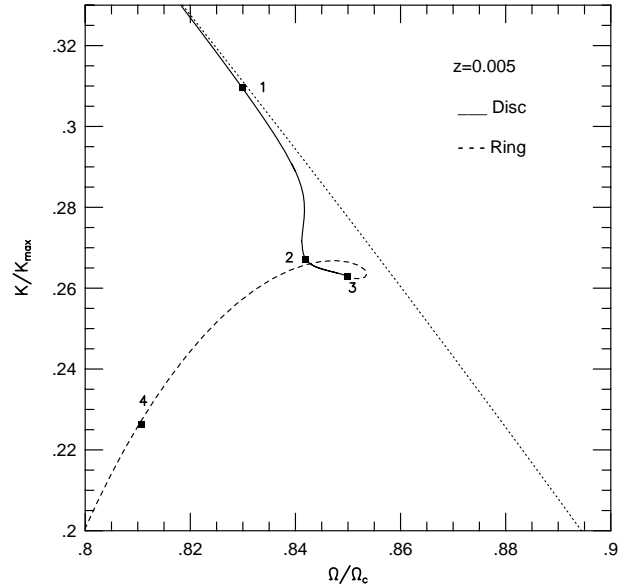

Figure 7. Pressure constant K versus angular velocity Ω given in units of the angular velocity of a dust disc Ω_c with the same central redshift. The solid line refers to a central redshift $z = 0.005$, and the dashed dotted line to $z = 0.22$. The other curves are labeled with the corresponding z values. The thin dotted line is the Newtonian limit (Maclaurin disc). The thick dotted line denotes the mass-shed limit. The values of Ω_c and K_{max} can be read off from Fig. 1 and Fig. 6.

relation (23) has a maximum at a finite redshift $z \approx 3.25$. The stronger relativistic cases have been calculated here using a higher grid resolution of 256×256. However, the last part of the curves for $z/(1+z) \gtrsim 0.9$ may nevertheless still be unreliable. The problem arises from the strong central concentration of the surface density (Fig. 4). Due to this problem M reaches its maximum for the first equation of state (20) most likely at infinite central redshift. At larger and larger redshifts, the density increasingly peaks at the origin (refer to the model with $z = 17.0$). The sequence terminates eventually at a black hole configuration, with all the mass located at the origin. The strong increase of internal pressure with z leads also to a central drop in the metric potential B which is plotted in Fig. 5. For the pressure-free dust disc, $B = 1$ everywhere; however, in the case of non-zero pressure, equation (28) creates a deviation from this simple relation. With increasing z, the metric potential B decreases (in all space) and its central value approaches zero in the extreme relativistic limit ($z = 1$). The variation of the polytropic constant K with redshift is displayed in Fig. 6. With increasing redshift, K drops from the Newtonian limit and increases again for stronger relativistic discs. Adding rotation ($\Omega > 0$) will lower the value of K. In the following diagrams K will be normalized to this maximum value K_{max}.

4.3 Rotating discs

Rotating discs were studied for the isentropic second equation of state only (23), and the primary results are displayed in Fig. 7 in the $K - \Omega$ diagram. The curves are labeled with the corresponding central redshifts of the sequences. Weaker relativistic discs (solid line, $z = 0.025$) follow the Newtonian curve (thin dotted line, eq. 24) closely up to a finite $\Omega < \Omega_c$ and then bifurcate continuously into a ring-like structure at

Figure 8. Enlargement of Fig. 7 displaying in detail the bifurcation from the disc to the ring configuration. The dotted line refers to the Newtonian disc solution. The solid line refers to the disc solution which turns into a ring structure (dashed line) at point 3. The corresponding surface density distributions at the marked locations are displayed in the next figure.
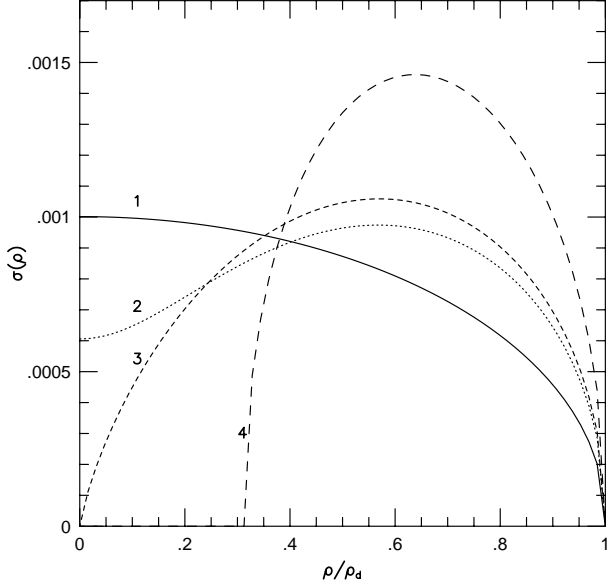
Figure 9. Plot of the surface density distribution versus radius at the locations marked in Fig. 7. Curve 1 follows closely the Newtonian curve

Figure 10. Detail of the bifurcation process for four different central redshifts (dashed line $z = 0.0005$; solid line $z = 0.005$, the others are given in plot). The Newtonian curve for the disc is given by the dotted line. The black squares mark the onset of the ring sequences (not plotted for $z = 0.015$).

$\Omega/\Omega_c \approx 0.84$. This continuous transition from disc to ring occurs only for $z \lesssim 0.01$. The details of the bifurcation process will be explained below. For intermediate central redshifts $0.01 < z < 0.22$ (dashed-dotted line), the discs and rings coexist with no apparent connecting branch between them. Stronger relativistic, $z \gtrsim 0.22$, (dashed lines) discs terminate in a mass shed limit, where at the outer edge of the disc ($\rho = \rho_\mathrm{d}$) gravity is balanced exactly by centrifugal forces. From the hydrostatic equation we obtain the criterion for reaching the mass-shed limit

$$U'_{,\rho} = \nu_{,\rho} - \frac{1}{2} \frac{v_{\varphi,\rho}^2}{1 - v_\varphi^2} = 0. \tag{39}$$

The end points of the dashed curves and the thick dotted line mark the loci where the edge of the disc reaches this limit. In case of the dust disc, all radii are at this limit simultaneously, since eq. (39) is exactly the hydrostatic equation for a pressure-less disc. It should be noted that the angular velocity reached in these stronger relativistic cases exceeds the value of the pressure-free case ($\Omega = \Omega_c$) for the same central redshift. This effect is caused by the non-linearity of the Einstein-equations. Through the gravitational action of the internal pressure, the potential B is then influenced, which in turn enters through the rotational velocity v_φ into the hydrostatic equation.

A more detailed view of the continuous bifurcation process is given in Fig. 8, which is an enlargement of the previous figure. The sequence bifurcates smoothly from the disc solution through a sequence of dumb-bell shaped density distributions which show a depression of the surface density in the middle region of the disc (see Fig. 9). At point 3 the density in centre has reached zero, and the ring structures begin. The numbers in Fig. 8 refer to the density distributions displayed in Fig. 9. The solid line in Fig. 9 follows approximately the Newtonian relation (25). With a growing inner ring radius the maximum surface density increases,
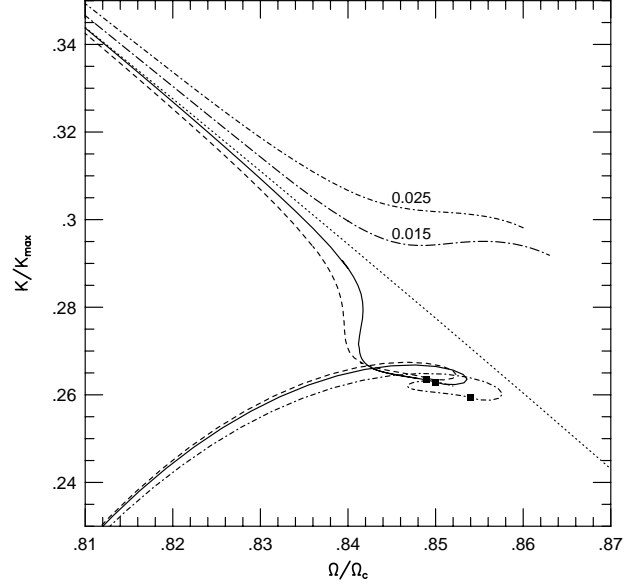
and the ring sequence turns eventually into a line with zero radial extent. These extreme ring models could not be obtained numerically, due to the lack of resolution.

At larger central redshifts, the bifurcation process changes its character; the discs and rings become disconnected. This is illustrated in Fig. 10, where the bifurcation regime in the $K - \Omega$ diagram is shown for three different values of z. At a critical value of z, which is given to the numerical accuracy by $z_\mathrm{c} \approx 0.01$, the connection between disc and ring is lost. Approaching z_c from below, the curves in the $K - \Omega$ diagram begin to be double valued until, upon reaching the critical point, they disconnect. Above z_c, the disc sequences do not join smoothly to the ring sequence but terminate instead at the mass-shedding limit. The ring sequences can still be continued somewhat into the dumb-bell regime but there the curve also terminates. Note that the apparent difference in the bifurcation curve for the weak relativistic limit and the Newtonian limit (see Kley 1996, Fig. 1) stems from the fact that here curves of constant central redshift (fixed central potential $\nu(0,0)$) were considered, while in the Newtonian work the curves are plotted for constant disc mass. The Newtonian line separates the two different regimes. Curves above end in the mass-shed limit, while curves below bifurcate continuously into a ring sequence. In Fig. 11 it is demonstrated that the disc sequences for $z > z_\mathrm{c}$, which terminate at the mass-shedding limit, start at that point where the rotational velocity v_φ at the outer rim ($\rho = \rho_\mathrm{d}$) coincides with the value of a pressure-less dust disc having the same central redshift. Above z_c, the rim-velocity lies always below that of the dust disc.

The total kinetic energy of the disc can be defined for rigid rotation by

$$T = \frac{1}{2} \Omega J. \tag{40}$$
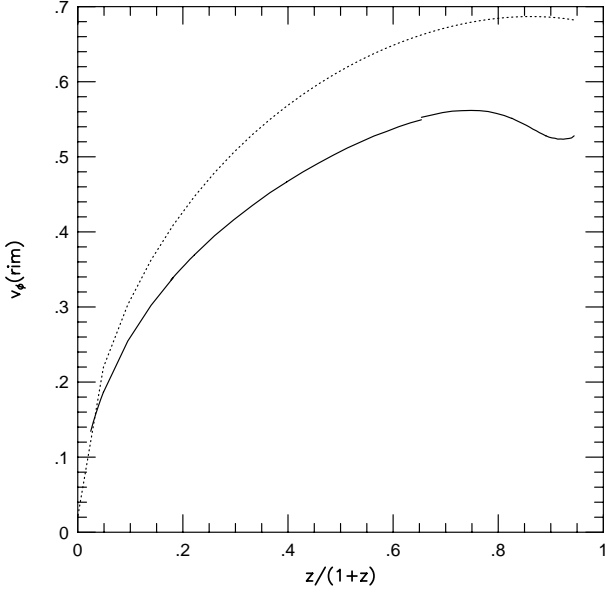
Figure 11. The rotational velocity at the rim ($\rho = \rho_{\rm d}$) of the disc as a function of central redshift for the dust disc (dashed line) and along the mass-shed limit (solid line). The curves join at the point where the disc begin to reach the mass-shed limit at $z = 0.22$.
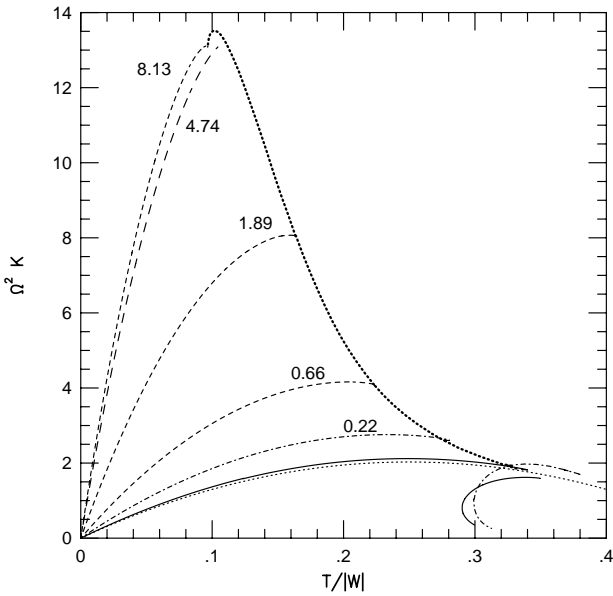
Figure 12. The normalized angular velocity versus the ratio of kinetic to potential energy for discs with different redshifts. The line types and the labeling corresponds to Fig. 7.

The total proper mass of the system, i.e. the energy of the configuration excluding gravitational potential energy and kinetic energy, can for the disc be defined as

$$M_{\rm p} = \int_{\rm disc} (\sigma^0 + \sigma^{\rm i}) u^t \sqrt{-g}\, {\rm d}^3 x. \tag{41}$$

The gravitational binding energy is then given by

$$W = M_{\rm p} + T - M. \tag{42}$$

In Fig. 12 the normalized angular velocity is plotted versus the ratio t of the kinetic energy to the gravitational binding energy, $t = T/|W|$. The Newtonian curve (thin dotted line) is given by the relation

$$\Omega^2 K = \frac{\pi^4}{6} t(1 - 2t), \tag{43}$$

which terminates at $t = 0.5$. For stronger relativistic discs the maximum possible t becomes smaller and smaller because the discs reach the mass-shed limit. For the weaker relativistic disc the curve for the mass-shed limit approaches the Newtonian limit tangentially.

5   CONCLUSION

We calculated the structure of uniformly rotating, infinitesimally thin, relativistic self-gravitating discs with internal pressure. The pressure is given by a polytropic equation of state. The polytropic exponent $\gamma = 3$ was used, since in this case there exists an exact solution in the Newtonian limit. This special choice corresponds to three-dimensional bodies of constant densities as well (see Hunter 1972). Thus, we may make a comparison of the results found here for flat discs with those of rotating, homogeneous relativistic stars. As Butterworth & Ipser (1976) showed, sequences of homogeneous, rotating relativistic stars usually terminate at the mass-shed limit. Close to the Newtonian case however, they were not able to follow the sequences to this limit. We suggest that, as weaker relativistic discs bifurcate into a ring, weaker relativistic stars of constant density bifurcate into a toroid structure as well, and do not end at the mass-shed limit. In the Newtonian limit, the structure of these constant density toroids were calculated by Eriguchi & Sugimoto (1981).

The pressure-less discs possess ergo-regions, where the dragging of inertial frames would force observers to rotate. These first appear at a single point within the disc at $z_{\rm e} = 1.41$ and reach the edge of the disc at $z = 1.89$ (Meinel & Kleinwächter 1993). They also occur in rotating stars (Butterworth & Ipser 1976). For discs with internal pressure however, we found no indication of the existence of ergo-regions. It is to be expected that there exists a continuous transition from the zero-pressure $K = 0$ case to discs with non-vanishing pressure (K small). However, this connection could not be demonstrated numerically, as disc sequences end either at the mass-shed limit or bifurcate into rings before reaching the pressure-less limit. One might speculate, perhaps, that such a connection can be achieved by a disc which consists of two parts: a pressure supported central region ($0 < \rho < \rho_{\rm p}$), surrounded by a dust disc ($\rho_{\rm p} < \rho < \rho_{\rm d}$). The dust disc would refer to $\rho_{\rm p} = 0$, and the disc sequences to $\rho_{\rm p} = \rho_{\rm d}$.

In some rotating relativistic stars, there are sequences of supra-massive stars (Cook, Shapiro & Teukolsky 1992), which are so massive that they exceed the rest mass of a non-rotating star, and can only exist for non-zero rotation. In the case of flat relativistic discs with non-zero internal pressure, we did not find any supra-massive disc sequences. Possibly, these negative results are a result of the particular equation of state where in the strong relativistic limit the

mass is always concentrated in the centre of the disc, as shown in Fig. 4 for the non-rotating case. Other relations between pressure and surface density, in particular a smaller γ, could also possibly lead to supra-massive sequences or ergo-regions.

The numerical method developed here is sufficiently general to be applied to the study of differentially rotating discs, and can easily be extended to three-dimensional rotating stars as well. This may be the subject of a future further investigation. A stability analysis of the computed equilibrium configurations lies beyond the scope of the present paper.

ACKNOWLEDGMENTS

REFERENCES

Bardeen J. M., Wagoner R. V., 1971, ApJ, 167, 359
Binney J., Tremaine S., 1987, Galactic Dynamics. Princeton University Press, New Jersey
Butterworth E. M., Ipser J. R., 1976, ApJ, 204, 200
Cook G. B., Shapiro S. L., Teukolsky S. A., 1992, ApJ, 398, 203
Eriguchi Y., Sugimoto D., 1981, Prog. Theor. Phys., 65, 1870
Hunter C., Ann. Rev. Ast. & Astrophys., 3, 219
Neugebauer G., Meinel R., 1993, ApJ, 414, L97
Neugebauer G., Meinel R., 1995, Phys. Rev. Lett., 75, 3046
Meinel R., Kleinwächter A., 1995, Einstein Studies 6, Birkhäuser (Boston), p339.
Kley W., 1996, MNRAS, 282, 234.
Pichon C., Lynden-Bell D., 1996, MNRAS, 280, 1007.
Turakulov Z.Y., 1990, Mod. Phys. Let. A, 5, 725.